Military Technical College
Kobry El-Kobbah,
Cairo, Egypt

8th International Conference
on Electrical Engineering
ICEENG 2012

Curvelet transform for water bodies extraction from high resolution satellite images

By

Mohamed Elhabiby* A. S. Elsharkawy** N. El-Sheimy***

Abstract:

In this research paper, a new implementation on the second generation curvelet transform in the edge detection of coastline is presented and applied on WorldView-2 imagery**,** together with a comparison with the classical edge detection methods such as Canny operator and the traditional wavelet transforms. This implementation is aiming to compare this new approach to the traditional edge detection techniques. It is found that the curvelet proposed implementation performs better in detecting larger and elongated structures compared to the Canny and the wavelet transforms. However, Although this method is promising and efficient for edge detection, the quality of the edge detection is still a function of the pre-processing steps (the classification step in this research paper) , as any edge detector will suffer from the heterogeneity of the images especially when using very high resolution imagery.

Keywords:

Curvelet transform, Wavelet transform, Edge Detection, High resolution satellite imagery.

---

* Ain Shams University, Cairo
** Egyptian Armed Forces
*** Dept. of Geomatics Engineering, University of Calgary, Calgary, Alberta

1. Introduction

Second generation curvelet transform provides optimally sparse representations of objects, which display smoothness except for discontinuity along the curve with bounded curvature [1]. Some papers have investigated this technique for edge detection in high resolution satellite imagery such as IKONOS or QuickBird, and microscopic imagery, [2-5] which show a great potentials of using curvelet transform in solving edge detection problems.

Urban studies, coastal erosion, and agricultural surveys are a few examples where edge detection can be utilized. In the past few years, the development of edge detection techniques for the analysis of multi-temporal remote sensing imagery has been intensively growing. For many years, satellite based remote sensing has been a priceless tool for change detection. No other platform can constantly revisit an area, quantify and classify land cover or land use on such a broad scale. Satellite imagery are proving to be a cost-effective alternative to aerial photography, especially, for the acquisition of Land Cover information[6].

One of the most important characteristic in an image is the features edges, which can be described as a discontinuity in the local domain of the image. These discontinuities may result as gray, colors and texture variations [4]. Edge detection has broad applications in the domain of image processing, computer vision and so on. The influence of this process comes from the fact that it is usually lies at the bottom of the classification process to serve as a base map for all other coming modules. Consequently, the more accurate this process is, the more accurate the whole classification results.

In this research paper an implementation of the second generation curvelet transform for edge detection will be introduced and a comparison with the optimal edge detector operator, Canny, will be done. In the following two sections, a brief introduction about Curvelet and Canny operator will be introduced followed by Data used description and methodology section, then the results and analysis section and finally the Conclusions.

2. The basics of curvelet transform

Initial introduction of Curvelet transform technique was originally introduced by Candes and Donoho in 1999 as a result of the increasingly demand in the presence of effective multi resolution analysis that has the ability to overcome the drawbacks of wavelet analysis. The transform was designed to represent edges and other singularities along curves much more efficiently than traditional transforms, i.e. using many fewer coefficients for a given accuracy of reconstruction [7]. This transform used a complex series of steps involving the ridgelet analysis of the radon transform of an image. However, the performance was considered slow.

Later and based on a frequency partition technique, the same authors proposed a considerably simpler second-generation curvelet transform. This second generation curvelet transform is meant to be simpler to understand and use. It is also faster and less redundant compared to its first generation version[8]. In the new version of curvelet the ridgelet transform was discarded, thus reducing the amount of redundancy in the transform and increasing the speed considerably. Curvelet transform is defined in both continuous and digital domain. Moreover, it can be used for multi-dimensional signals. Since image-based feature extraction requires only 2D FDCT, The discussion will be focused on only two dimensional application and implementation[1].

2.1 Continuous-time Curvelet Transforms

The curvelet representation in two dimensions continuous space, i.e., R^2, will be through spatial variable x, with ω a frequency domain variable, and with r, θ polar coordinates in the frequency domain. Then, a pair of windows function *W(r)* and *V(t)* *i*s introduced , the "radial window" and "angular window" respectively. These windows will obey the admissibility conditions:

$$\begin{cases} \sum_{j=-\infty}^{\infty} W^2(2^j r) = 1 & , r \in (\frac{3}{4}, \frac{3}{2}) \\ \sum_{l=-\infty}^{\infty} V^2(t-l), & t \in (-\frac{1}{2}, \frac{1}{2}) \end{cases} \quad (1)$$

Where *j* is a radial variable and *l* is an angular variable. The frequency window in the Fourier domain is defined by:

$$2^{-\frac{3j}{4}} W(2^{-j} r) V\left(\frac{2^{\lfloor j/2 \rfloor}\theta}{2\pi}\right) \quad (2)$$

Where $\lfloor j/2 \rfloor$ is the integer part of *j*/2

In the spatial Cartesian domain, the scaling of the radial window introduces an angular window with short axis with 2^{-j}, and a long axis with $2^{-j/2}$. *T*herefore, the effective length and width obey the anisotropy scaling relation width ≈ length^2, and U_j is a polar wedge window, as show in Figure 1.

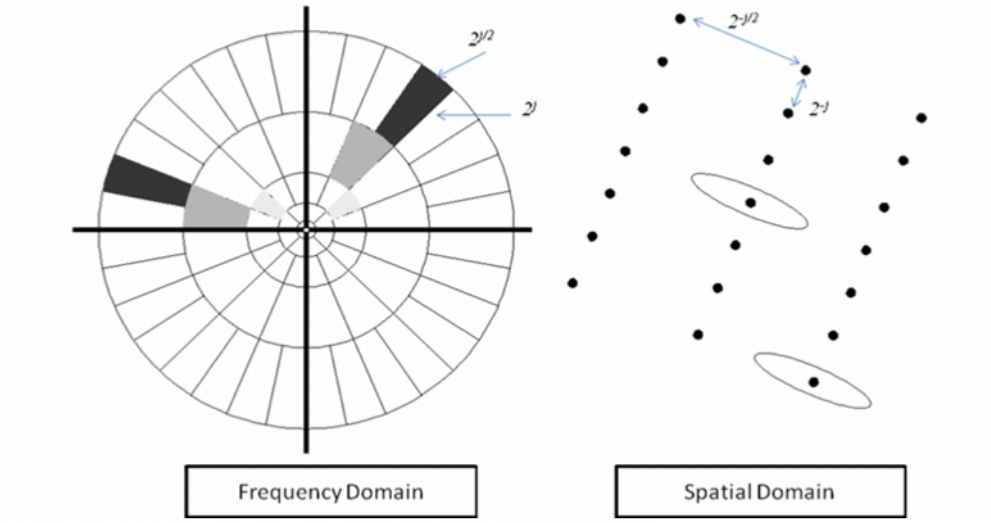

Figure 1. *Curvelets in Fourier frequency (left) and spatial domain (right)[1]*

In the frequency domain, the curvelet coefficient, with the j scale, the *l* angle and the sequence of translation parameters $k = (k_1,k_2) \in Z^2$, is defined as:

$$C(i,j,k) := \frac{1}{(2\pi)^2} \int \hat{f}(\omega) U_j(R_\theta \omega) e^{i(x_k^{(j,l)},\omega)} d\omega \qquad (3)$$

Figure 1 illustrates the result of partitioning the Fourier plane into radial (concentric circles) and angular divisions. The concentric circles are responsible for the decomposition of an image into multiple scales, *j*, while the angular divisions partition the band passed image into different angles or orientations *l*[4]. For instance the light gray wedges represent the maximal support of the curvelet function $\hat{\varphi}$ (3,2,k) and $\hat{\varphi}$ (3,7,k), while the gray wedges represent $\hat{\varphi}$ (4,3,k) and $\hat{\varphi}$ (4,8,k) and the dark wedges represent $\hat{\varphi}$ (5,5,k) and $\hat{\varphi}$ (5,15,k). As a result, defining the scale *j* and angle *l* is the proper way to deal with a particular wedge. By noticing the spatial domain, Figure 1 right, it was foundthat each of the wedges corresponds to a specific curvelet, shown as ellipses, at a given scale and angle. This indicates that the curvelet coefficients for that scale and angle can be determined by the inverse FFT of this particular wedge [3]. This is the main idea behind the implementation of curvelet transform. As shown in Figure 1, curvelets have a well localized, needle-shaped in higher scales, as the wedges are longer and thinner with scale growing [8].

2.2 Discrete Curvelet Transform

Coronae and rotations, as in the continuous-time definition, are not especially adapted to Cartesian arrays, so it is convenient to replace these concepts by Cartesian equivalents; here, “Cartesian coronae” based on concentric squares (instead of circles) and shears.

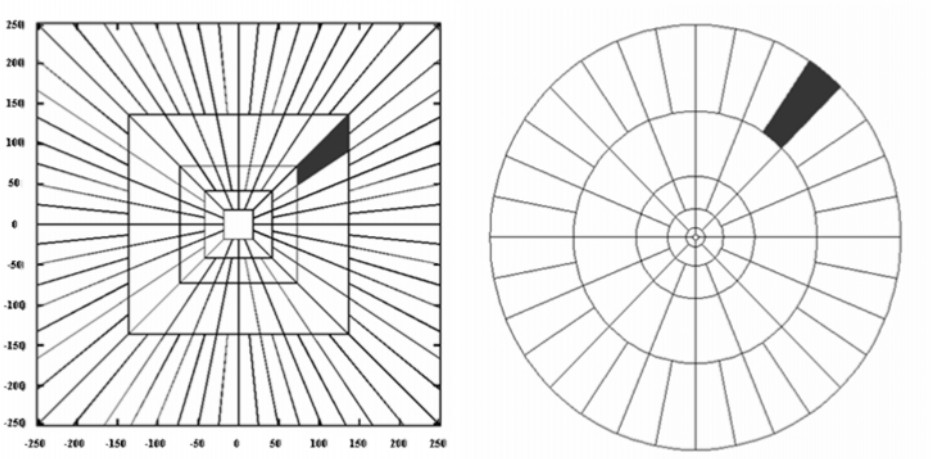

***Figure 2**. The transition from the continuous-time definition (left) to the discrete-time definition(right) [1].*

The above figure (left) illustrates the basic digital tiling where, the windows ˜U_j` smoothly localize the Fourier transform near the sheared wedges obeying the parabolic scaling. The shaded region represents one such typical wedge.
Now the Cartesian window $\widetilde{U}$ is defined as:

$$\widetilde{U}_{j,l}(\omega) := \widetilde{W}_j(\omega) V_j(S_{\theta i}\omega) \tag{4}$$

Where:

$$\begin{cases} W_j(\omega) = \sqrt{\phi_{j+1}^2(\omega) - \phi_j^2(\omega)}, \\ V_j(\omega) = V\left(\frac{2^{\lfloor \frac{j}{2} \rfloor}\omega_1}{\omega_2}\right) \end{cases} \tag{5}$$

Φ is defined as the product of low-pass one dimensional windows:

$$\phi_j(\omega_1, \omega_2) = \phi(2^{-j}\omega_1)\phi(2^{-j}\omega_2) \tag{6}$$

And S_θ is the shear matrix:

$$S_\theta := \begin{pmatrix} 1 & 0 \\ -tan\theta & 1 \end{pmatrix} \tag{7}$$

Hence, the discrete curvelet coefficients are defined as:

$$C(i,j,k) := \int \hat{f}(\omega)\widetilde{U}_j(S_{\theta l}^{-1}\omega)e^{i(S_{\theta l}^{-T}, \omega)}d\omega \tag{8}$$

According to [1], there are two different digital implementations of FDCT:

- Curvelets via **USFFT** (Unequally Spaced Fast Fourier Transform)
- And Curvelets via **Wrapping**.

Both the variants are linear and take as input a Cartesian array to provide an output of discrete coefficients. The only difference is in the choice of the spatial grid where curvelets at each scale and angle are translated. As the FDCT wrapping is the fastest curvelet transform currently available [9], the wrapping version of curvelet transform, will be used in the implementation. The FDCT wrapping algorithm may be summarized as follow:

1. Take FFT of the image
1. Divide FFT into collection of Digital Corona Tiles as in (Figure 2)
2. For each corona tile do the following
   - Translate the tile to the origin as in (Figure 3)
   - Wrap the parallelogram shaped support of the tile around a rectangle centered at the origin as in (Figure 4).
   - Take the Inverse FFT of the wrapped support
   - Add the curvelet array to the collection of curvelet coefficients.

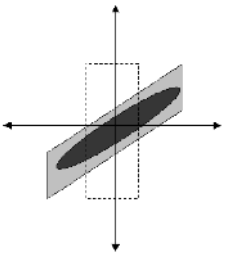

Figure 3. *Support of Wedge before Wrapping*

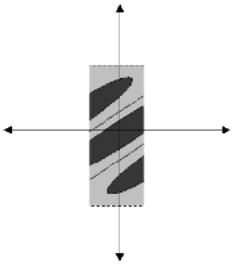

Figure 4. *Support of Wedge after Wrapping*

The values of curvelet coefficients are depending on how they are aligned in the real image. One can expect higher coefficients values when the curvelet is accurately aligned with a given curve in an image. A very clear explanation is provided in Figure 5. The curvelet named ‘c’ in the figure is almost perfectly aligned with the curved edge and therefore has a higher coefficient value. Curvelets ‘a’ and ‘b’ will have coefficients close to zero as they are quite far from alignment with the curve [3]. From the previous discussion it is clear that the curvelet transform provide a distinguished characteristic for the signals where they are better localized in both frequency and spatial domain compared to wavelet or any other transform.

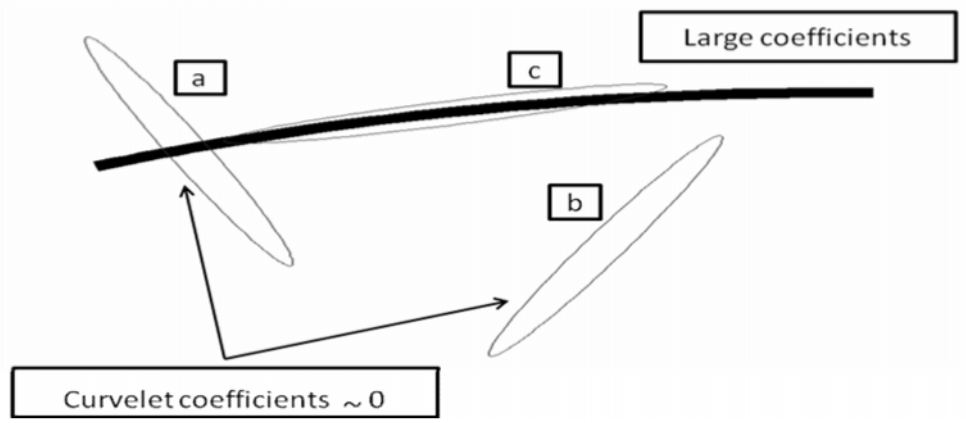

***Figure 5**. Alignment of curvelets along curved edges[3]*

The unique mathematical property to represent curved singularities in a non-adaptive manner makes the Curvelet transform as a higher dimensional generalization of wavelets.

The main advantage of the curvelet transform over wavelet is that the edge discontinuity is better approximated by curvelets than wavelets. Curvelets can provide solutions for the limitations the wavelet transform suffers from, which can be summarized as follow:

- Curved singularity representation,
- Limited orientation (Vertical, Horizontal and Diagonal)
- And absence of anisotropic element (isotropic scaling)

If an image function f is approximated by largest *m* coefficients as $\hat{f}_m$, then the approximation errors are given by:

$$\left\| f - \hat{f}_m^F \right\|^2 \propto m^{-1/2},\ m \to +\infty \qquad \text{Fourier transform}$$

$$\left\| f - \hat{f}_m^W \right\|^2 \propto m^{-1},\ m \to +\infty \qquad \text{Wavelet transform}$$

$$\left\| f - \hat{f}_m^C \right\|^2 \propto m^{-2} \log(m^3),\ m \to +\infty \qquad \text{Curvelet transform}$$

Figure 6. shows the edge representation capability of wavelet (left) and curvelet transform (right). More wavelets are required for an edge representation using the square shape of wavelets at each scale, compared to the number of required curvelets, which are of elongated needle shape.

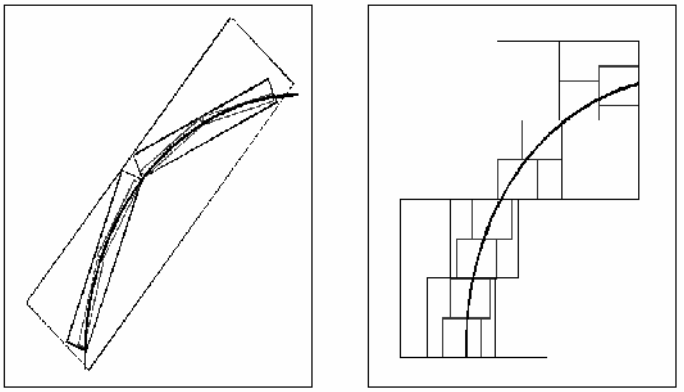

***Figure 6**. Representation of curved singularities using wavelets (right) and curvelets (left)[3].*

2.3 canny operator

Canny edge detection is best known as the optimal edge detector operator for step edges detection. Canny used three criteria to design his edge detector.

- Reliable detection of edges with low probability of missing true edges, and a low probability of detecting false edges.
- The detected edges should have a minimum distance to the true location of the edge.
- There should be only one response to a single edge (thin lines for edges)[10].

Based on these criteria, the canny edge detector first smoothes the image to eliminate any noise, then it finds the image gradient to highlight regions with high derivatives. The regions with high derivatives are tracked by the algorithm to suppress any pixel that is not at the maximum (non-maximum suppression). The remaining pixels are further reduced by two thresholds T1 and T2. If the magnitude is below T1, it is set to zero (none edge), if the magnitude is above T2, it is made an edge. And if the magnitude is between the two thresholds, then it is set to zero unless there is a path from this pixel to a pixel with a gradient above T2[10, 11].

The algorithm runs in 5 steps:

1. **Smoothing**: Blurring of the image to remove noise.
2. **Finding gradients**: The edges should be marked where the gradients of the image have large magnitudes.
3. **Non-maximum suppression**: Only local maxima should be marked as edges.
4. **Double thresholding**: Potential edges are determined by thresholding.
5. **Edge tracking by hysteresis**: Final edges are determined by suppressing all edges that are not connected to a very certain (strong) edge.

3. Data and method

Data used

WorldView-2 is the first commercial high-resolution satellite to provide 8 spectral sensors in the visible to near-infrared range. Each sensor is closely focused on a

particular range of the electromagnetic spectrum, which is sensitive to a specific feature on the ground. In concert, they are designed to improve the segmentation and classification of land and marine features, [12]. Figure 7 presents a quick comparison between QuickBird, IKONOS, GeoEye-1 and WorldView-2 regarding their spectral and panchromatic bands.

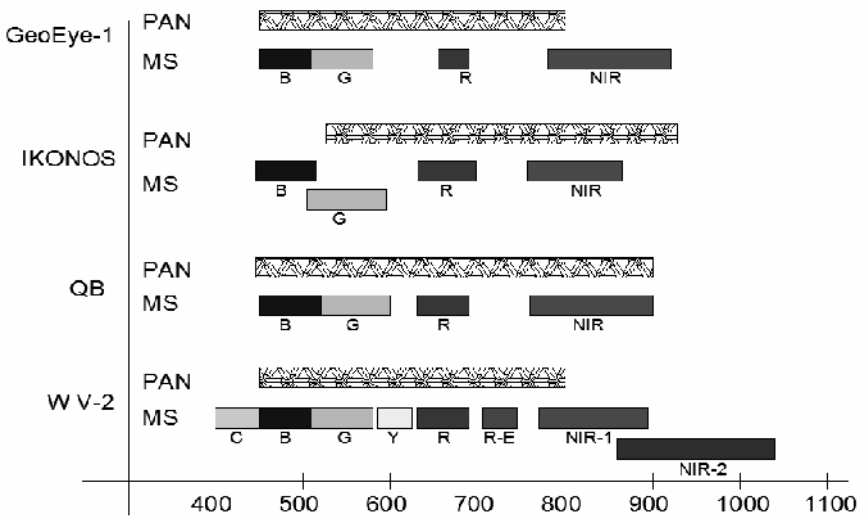

***Figure 7**. Comparison between spectral band coverage of WV-2, QB, IKONOS and GeoEye*-1[13]

Multispectral imagery has provided great value in helping to understand the earth and the impacts of natural processes and man-made activities. Higher resolution multispectral satellites with traditional visible to near infrared (VNIR) bands are able to separate fine scale features, with spatial resolutions of 0.5-1 meter, for example, discriminating between grasses vs. trees, segmenting urban areas by housing types, and discriminating between types and condition of roads,[12]. The high spatial resolution together with the increased spectral resolution of WorldView-2, will grant the additional data necessary to tackle the challenge of feature classification. Overall improvement in classification accuracies were observed when simulated WorldView-2 8-band imagery were used,[12].

For example, when looking at land classes, the improvement in accuracy compared with traditional VNIR imagery is expected to deliver a 10-30%. Specifically, the improvement of accurately classified roads was increased from 55% to over 80%. The increased sensitivity to plant material and soil types provided by the addition of the Red-Edge, Yellow and NIR2 bands are the reason behind these striking improvements. Also, the classification of water bodies is expected to improve with more than 5% better than the medium resolution satellite imagery,[12] . The quality of automated classification techniques is also expected to increase as a result of the increased spatial resolution of WorldView-2. The next table will summarize the role of each spectral band.

Table 1. The role of each spectral band,[12]

Band	**Characteristics**
Coastal Blue (400-450 nm)	New band /least absorbed by water/ Absorbed by chlorophyll in healthy plants
Blue (450-510 nm)	Provides good penetration of water/ Less affected by atmospheric scattering and absorption.
Green (510-580 nm)	Ideal for calculating plant vigour and plants types when used in conjunction with the Yellow band
Yellow (585-625 nm)	New band/Very important for feature classification
Red (630-690 nm)	Very important band for vegetation Discrimination/Very useful in classifying bare soils, roads, and geological features
Red-Edge (705-745 nm)	New band/Very valuable in measuring plant health and aiding in the classification of vegetation
NIR1 (770-895 nm)	Separates water bodies from Vegetation/ identifies types of vegetation / discriminates between soil types
NIR2 (860-1040 nm)	New band/ less affected by atmospheric influence/Enables broader vegetation analysis.

Study area

The study area is a residential area in Ismailia city about 120 Km to the north east direction from Cairo the capital of EGYPT. The study area is an urban area comprises scattered buildings, two shorelines and water body. The data was provided by Digital Globe, http://www.digitalglobe.com, the images was captured on April 7th, 2011 in morning time. Figure 8 illustrates a false color composite, NIR-2 G B, of the study area.

4. Methodology

Basic spectral information for mapping applications such as land-use surveys are essentially provided by the multispectral bands. However, as the limitation to the data storage volume and transmitting capability of the satellite, satellites do not collect high-resolution multispectral images directly. So, what happen is the sensor collects only one panchromatic band, wide range of spectrum, with higher spatial resolution and the rest of the bands, with narrower ranges of the spectrum, with lower resolution[14]. In case of WorldView-2 the panchromatic band volume is twice as the whole 8-spectral bands together. Considering these limitations, it is clear that effective image fusion techniques are the most effective solution for providing high-spatial-resolution and high-spectral-resolution remote sensing images.

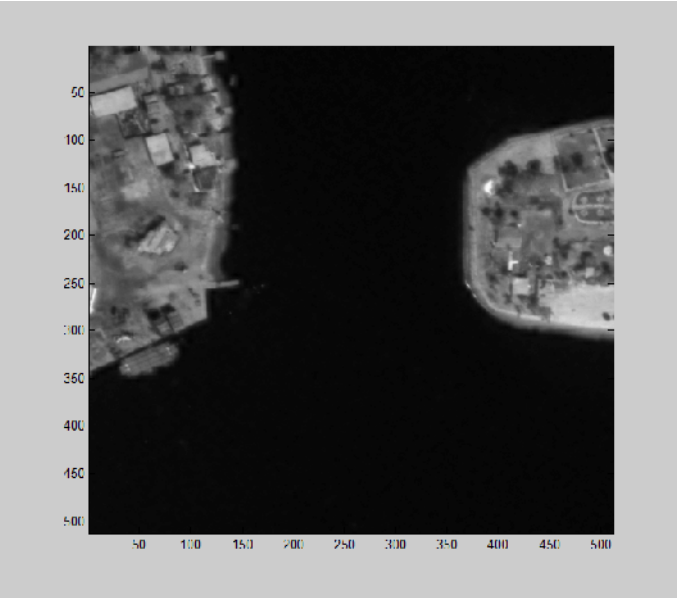

***Figure 8**. Gray scale image of the area of study*

The proposed algorithm begins with a data fusion between the panchromatic band of the WorldView data, 0.50 m, and the multispectral ones, 2.00 m resolution, to generate 8-spectral bands with a resolution of 0.50 m. One of the most common fusion techniques is the Brovey Transform. This technique is optimum when increase in contrast in the low and high ends of an images histogram (i.e., to provide contrast in shadows, water, and high reflectance areas such as urban features) is needed. The procedure of this transform starts with multiplying each MS band by the high-resolution PAN band, and then divides each product by the sum of the MS bands. Since the Brovey Transform is intended to produce RGB images, only three bands at a time should be merged from the input multispectral scene[14] in our case NIR-2 is chosen, Green and Blue bands.

Based on the curvelet transform theory a new implementation for detecting edges will be introduced depending on the fact that the values of curvelet coefficients are determined by how they are aligned in the real image, the more accurately a curvelet is aligned with a given curve in an image, the higher is its coefficient value. Analyzing these coefficients, it can be found that the coefficient in each scale level contains different information. Consequently, by arranging the coefficients of each level and take the most significant part of them, this will enhance the edge information that represents the important part of the image to us. Then, the coefficients are reconstructed to get a new image where the edge parts are enhanced.

Morphological filters will be applied to eliminate the undesired noised pixels. Figure 9 represent a schematic diagram of the aforementioned algorithm.

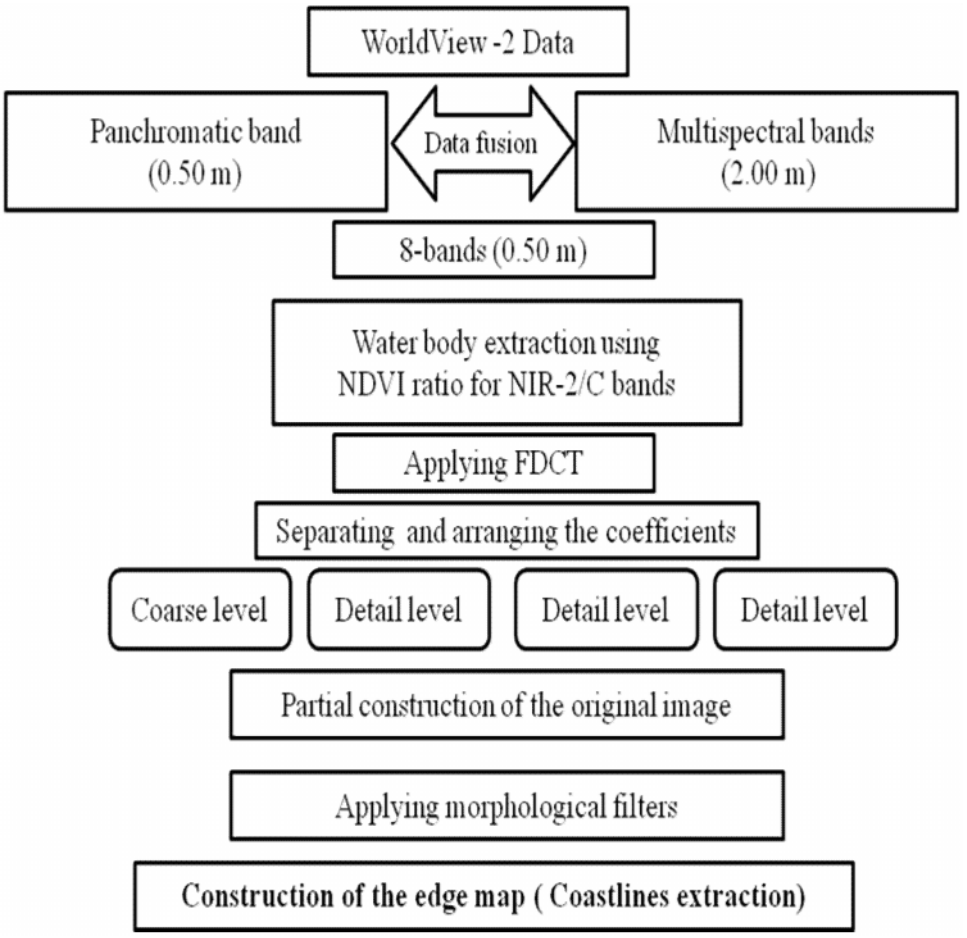

Figure 9. *The proposed algorithm*

*5. **Results and Discussion***

The proposed algorithm is mainly depending on the curvelet transform with pre-processing steps. The pre-processing steps involve data fusion between the multispectral bands with 2.00 m resolution with the panchromatic band with 0.5 m resolution.

NDVI rationing between bands 8 and 1 is then applied to extract the water body. Then, soft thresholding is applied to the NDVI output to get binary image as in Figure 10.

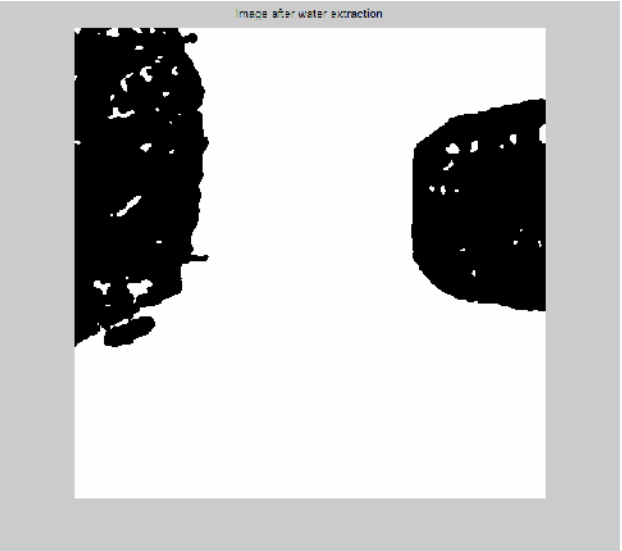

***Figure 10**. The image after water extraction*

Then, the 2D FFT of the output image is calculated to obtain Fourier samples. And according to the size of the original image the scale levels are determined following the law $\boldsymbol{n=\log_2(N)-3}$, where N is the minimum number of the image size and n is the number of the scale levels, i.e. for N=512 pixels the n=6 levels . These scale levels are divided into three parts, which are coarse level, detail level and fine level. Then curvelet transform is applied to extract the coefficients from these parts. Images are then reconstructed for each level with those coefficients as in Figure 11. First scale generates the coarse level image, while second and third scales were merged to generate the detail level 1 image, fourth and fifth scales were merged to generate the detail level 2 image and finally sixth scale was responsible for the generating of the detail level 3 image.

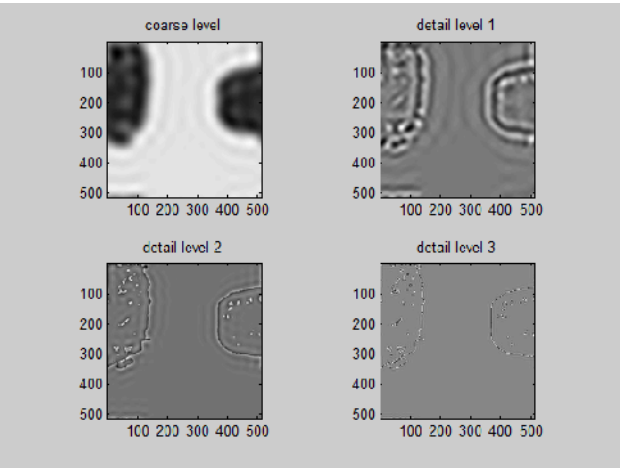

***Figure 11.** The reconstructed coarse and fine details levels*

Analyzing the coefficient of curvelet, it can be found that the coefficient in each scale level contains different information. Consequently, by arranging the coefficients of each level and take the most significant part of them, this will enhance the edge

information that represents the important part of the image to us. Then, the coefficients are reconstructed to get a new image called the edge map, as in Figure 12, where the edge parts are enhanced. Table 2 summarizes the total number of coefficient in each scale and the actual used percentage.

***Table 2**. The percentage used in reconstructing the edge map image*

Scale	No. of total coefficients	Percentage used	No. of used coefficients
1	441	0%	0
2	5984	0%	0
3	22880	0%	0
4	90144	100%	90144
5	357408	1%	3574
6	1417248	1%	14172
Total	1894105	5.7 %	107890

The edge map is then thresholded to get enhanced edge map as in Figure 13. The reconstructed edge image was thresholded based on the fact that the strong edges have abrupt changes in the pixel from negative to positive values and the absolute summation falls within a certain threshold.

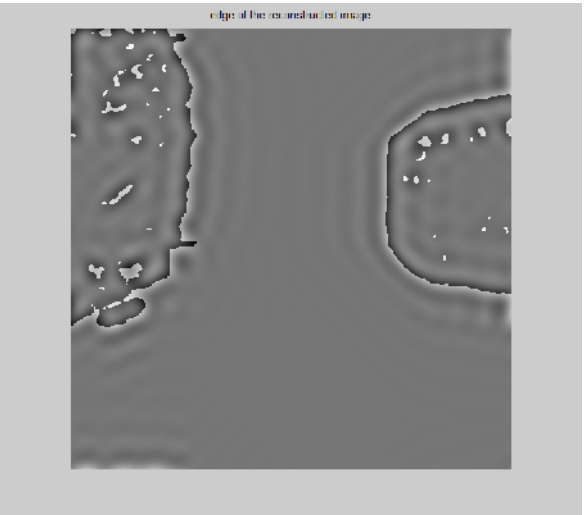

***Figure 12**. The reconstructed edge map*

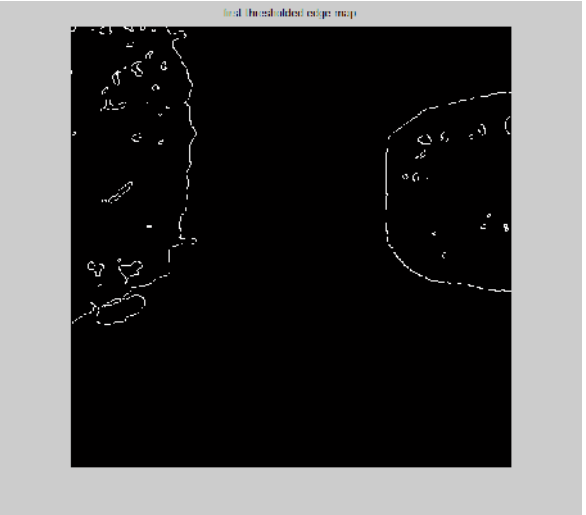

Figure 13. *The reconstructed edge map after thresholding*

The next step is applying morphological filters to clear the undesired artefacts and the result is in Figure 14.

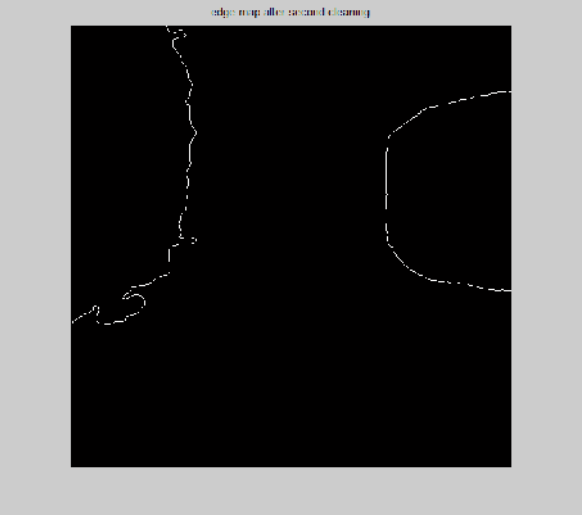

Figure 14. *The reconstructed edge map after applying morphological filters*

The final result was overlaid over the original image to show the exact matching of the delineation of the coastline.

Figure 15 *final result overlaid over the original image*

To illustrate the quality of this algorithm compared with Canny and wavelet transforms, the procedure was repeated using these two methods and the final result is in Figures 16, 17 and 18. Canny was used with sigma equal to 1 and the thresholds T1= 0.006 and T2= 0.02.

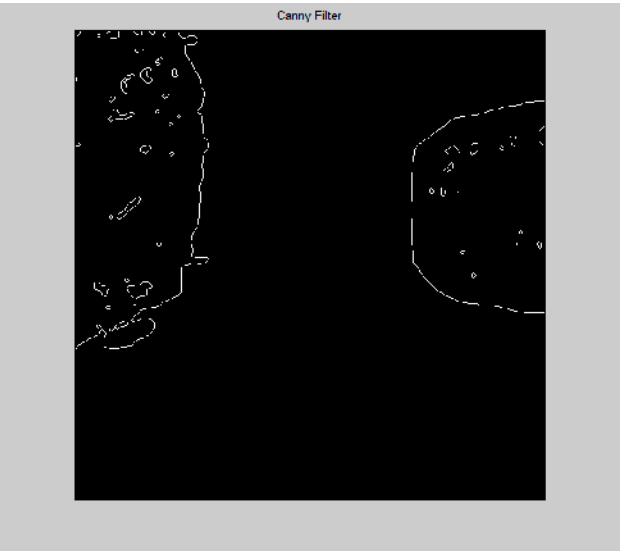

Figure 16 *results with Canny Operator (the input is the classified image)*

The result above shows almost identical similarity with the curvelet transforms edge detection result, when the input to Canny was the classification image (Figure 10). While if the input was the original image without any classification the result was as in the next figure.

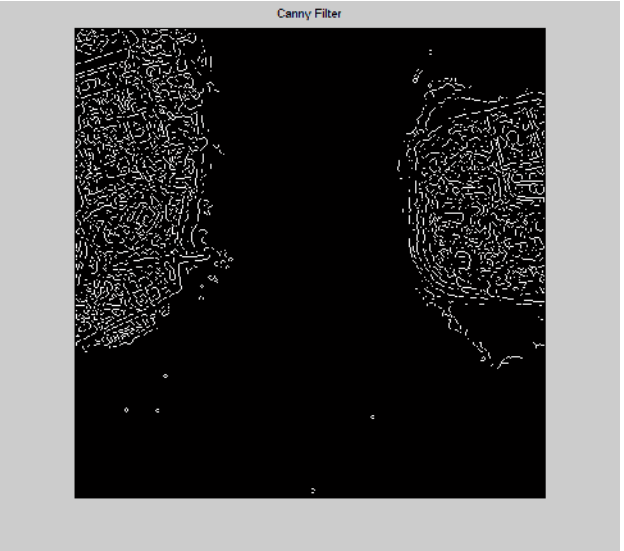

***Figure 17** results with Canny Operator (the input is the original image)*

The case was different with the wavelet as in the Figure 18, which illustrate the edge detection result when using the classified image as an input to the wavelet transform. And it was much worse when using the original image as an input to the transforms. The total number of generated coefficients was 262144 and it was used totally, which is more than twice the number of coefficients used in case of curvelet.

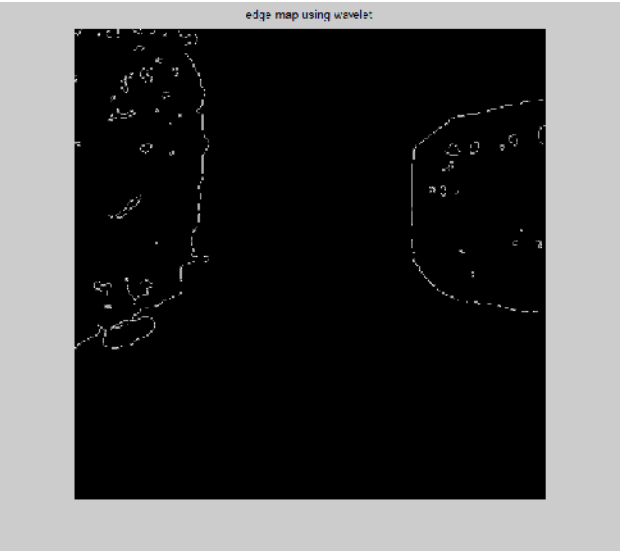

***Figure 18** results with Wavelet transform (the input is the classified image)*

A small area in the classification map, figure 10, was picked and enlarged to emphasize the potentials of using the curvelet transform as an edge detector against Canny and wavelet transform. Figure 19 is highlighting one pixel in every edge map and in the original classification map as well.

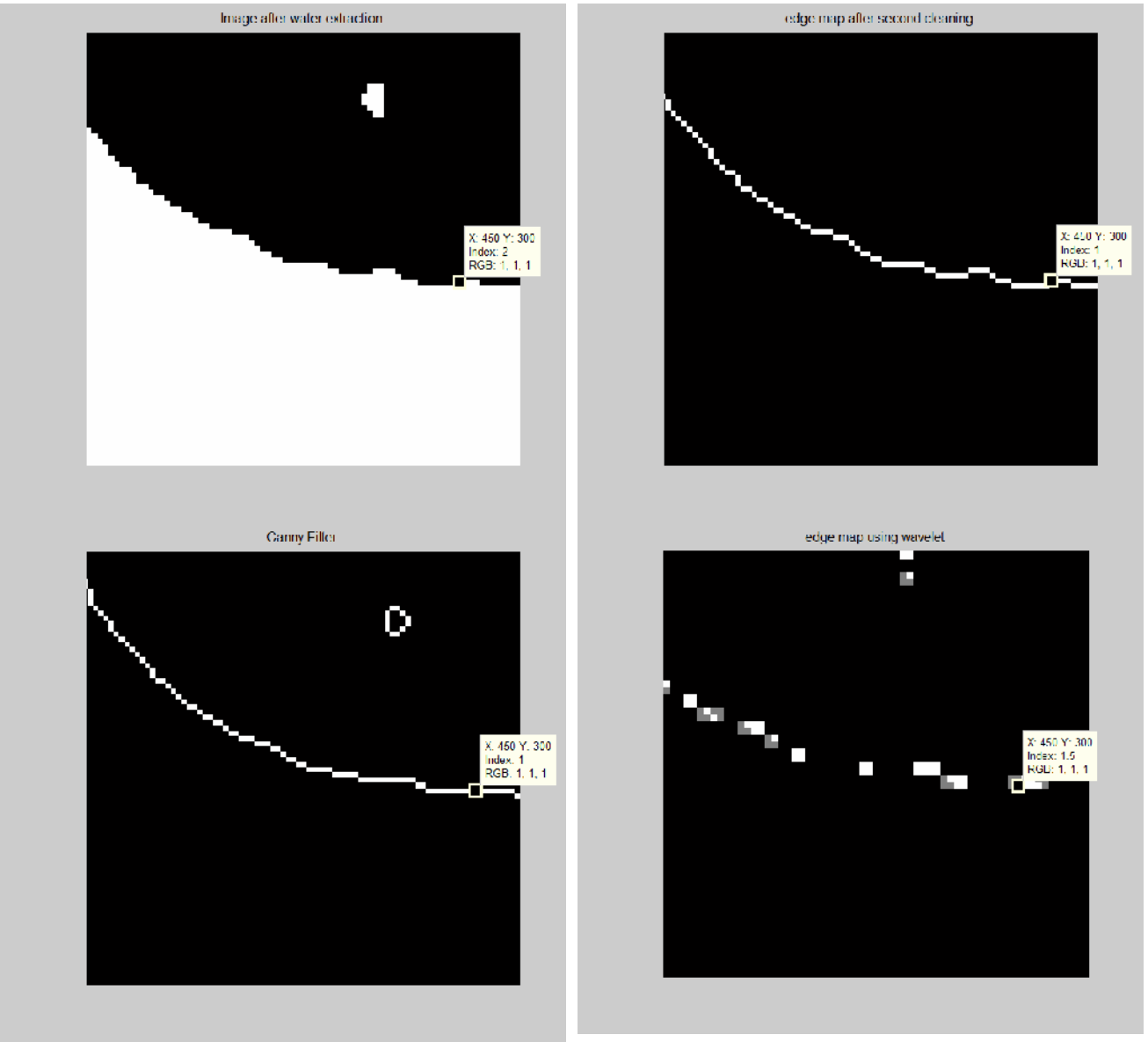

Figure 19 *highlighting a certain pixel in curvelet , Canny and wavelet transform*

It was very clear that curvelet gave the most accurate delineation of the edges better than the Canny and the wavelet transform.

6. Conclusions

In this research paper, the proposed implementation relied on the fact that the values of curvelet coefficients are determined by how they are aligned in the real image. As, the more accurately a curvelet is aligned with a given curve in an image, the higher is its coefficient value. Consequently, the image is enhanced by using different method to process different scale level coefficient where each level of coefficient separately contains the information about different frequency domain of the image. The method is composed of some primary steps, such as classification step of the required feature, water in this case. Then curvelet transform is applied, coefficient manipulation, invert

transform, edge enhancement, and morphological filters. The proposed implementation showed good results for detecting larger and elongated structures curves compared to wavelet transform and Canny operator.

The proposed algorithm was applied with high resolution and the results were promising, putting in mind the great enhancement in the spectral and spatial resolutions provided by WorldView-2 satellite. These enhancement were reflected on the quality of classification and the dimensions of the detected objects

WorldView-2 with the new Coastal Blue and NIR-2 gives excellent delineation of water bodies.

The total number of coefficients used to reconstruct the edge map using curvelet transform was 107890, 5.7% of the total coefficients, While in case of wavelet the coefficients was 262144, 100% of the total coefficients.

Although this method is promising and efficient for edge detection, there is one drawback must be regarded in the future, which one is that the quality of the edge detection is a function of the pre-processing steps (the classification step here), as any edge detector will suffer from the great deal of heterogeneity of the images especially when using very high resolution imagery, which will be the motivation for further investigation in the near future.

7. References

[1] E. Candes, *et al.*, "Fast discrete curvelet transforms," *Multiscale Modeling & Simulation*, vol. 5, pp. 861-899, 2006.

[2] T. Geback and P. Koumoutsakos, "Edge detection in microscopy images using curvelets," *BMC Bioinformatics*, vol. 10, p. 75, 2009.

[3] T. Guha and Q. M. J. Wu, "Curvelet Based Feature Extraction," in *Face Recognition*, M. Oravec, Ed., ed: InTech, Available from: http://www.intechopen.com/articles/show/title/curvelet-based-feature-extraction, 2010, pp. 35-46.

[4] L. Zhenghai and Q. Jianxiong, "Study of Technique of Edge Detection Based on Curvelet Transform," in *Second International Symposium on Computational Intelligence and Design*, 2009, pp. 543-545.

[5] M. Xiao, *et al.*, "Edge Detection of Riverway in Remote Sensing Images Based on Curvelet Transform and GVF Snake," presented at the Spatial Accuracy Assessment in Natural Resources and Environmental Sciences, Shanghai, P. R. China, , 2008.

[6] Y. O. Ouma, *et al.*, "Urban features recognition and extraction from very-high resolution multi-spectral satellite imagery: a micro–macro texture determination and integration framework," *IET Image Processing*, vol. 4, p. 235, 2010.

[7] D. L. Donoho and M. R. Duncan, "Digital curvelet transform: Strategy, implementation and experiments," in *Wavelet Applications Vii*. vol. 4056, H. H. Szu, *et al.*, Eds., ed, 2000, pp. 12-30.

[8] J. Ma and G. Plonka, "Computing with Curvelets: From Image Processing to Turbulent Flows," *Computing in Science and Engg.*, vol. 11, pp. 72-80, 2009.

[9] E. J. Candes and D. L. Donoho, "Continuous Curvelet Transform - I. Resolution of the wavefront set," *Applied and Computational Harmonic Analysis*, vol. 19, pp. 162-197, Sep 2005.

[10] J. Canny, "A Computational Approach to Edge Detection," *Pattern Analysis and Machine Intelligence, IEEE Transactions on*, vol. PAMI-8, pp. 679-698, 1986.

[11] B. Green. (2002, 20 April). *Canny Edge Detection Tutorial*. Available: URL: http://www.pages.drexel.edu/~weg22/can_tut.html

[12] D. Globe. (2009, the Benefits of the 8 Spectral Bands of WorldView-2. *White Paper*, 12.

[13] A. Elsharkawy, *et al.*, "A modified parallelepiped-like method for supervised classification for high resolution satellite imagery " presented at the CGU Annual Scientific Meeting, Banff, Calgary, 2011.

[14] K. G. Nikolakopoulos, "Comparison of nine fusion techniques for very high resolution data," *Photogrammetric Engineering and Remote Sensing*, vol. 74, pp. 647-659, May 2008.